Zitierweise: *Angew. Chem. Int. Ed.* **2025**, e202421234
doi.org/10.1002/anie.202421234

Systems Chemistry **Hot Paper**

Catalysis-driven Active Transport Across a Liquid Membrane

*Kaiyuan Liang, Federico Nicoli[+], Shaymaa Al Shehimy[+], Emanuele Penocchio, Simone Di Noja, Yuhan Li, Claudia Bonfio, Stefan Borsley, and Giulio Ragazzon**

Abstract: Biology has mastered energy transduction, converting energy between various forms, and employing it to drive its vital processes. Central to this is the ability to use chemical energy for the active transport of substances, pumping ions and molecules across hydrophobic lipid membranes between aqueous (sub)cellular compartments. Biology employs information ratchet mechanisms, where kinetic asymmetry in the fuel-to-waste (i. e., substrate-to-product) conversion results in catalysis-driven active transport. Here, we report an artificial system for catalysis-driven active transport across a hydrophobic phase, pumping a maleic acid cargo between aqueous compartments. We employ two strategies to differentiate the conditions in either compartment, showing that active transport can be driven either by adding fuel to a single compartment, or by differentiating the rates of activation and/or hydrolysis when fuel is present in both compartments. We characterize the nonequilibrium system through complete kinetic analysis. Finally, we quantify the energy transduction achieved by the catalysis-driven active transport and establish the emergence of positive and negative feedback mechanisms within the system.

Introduction

The conversion of chemical energy into transmembrane gradients through catalysis is fundamental to life.[1] Membrane proteins, such as Complex I, III and IV in the electron transport chain, use high-energy substrates[2] to generate transmembrane (proton) gradients, which in turn are used to drive adenosine triphosphate (ATP)[3] synthesis or metabolite transport.[4] Cells employ catalysis-driven information ratchet mechanisms[5–8] to transduce energy stored in kinetically stable, yet thermodynamically activated, substrates[2] (also called chemical fuels[9]), to pump concentration gradients. Catalysis of fuel-to-waste (i. e., substrate-to-product) reactions by membrane-spanning biomolecular pumps actively enables the transport of a cargo across a membrane.[10–15] The rates of ATP binding and release depend on the conformational state of the transmembrane pump[16] and thus result in kinetic asymmetry in the reaction cycle.[7,8,17–19]

Membrane transport can be divided into passive (Figure 1a) and active (Figure 1b,c) processes.[20] Passive transport involves the thermodynamically downhill relaxation of a cargo concentration towards equilibrium (Figure 1a). Active transport requires an energy input to drive a cargo concentration away from equilibrium. Active transport processes can be further divided into primary and secondary active transport.[20] Secondary active transport does not involve catalysis of a chemical reaction: the concentration of a co-transported substance relaxes to equilibrium, driving the cargo concentration away from equilibrium (Figure 1b).[21–25] In contrast, primary active transport relies on an orthogonal energy-providing process, such as light irradiation[26–32] or a fuel-to-waste reaction (Figure 1c). The nonequilibrium nature of active transport processes requires a ratchet mechanism for the transduction of energy.[7,8,33]

The very limited examples of transmembrane primary active transport in artificial systems are dominated by light-driven systems. Photoswitches illuminated with different wavelengths on either side of a membrane can result in active transport through selective uptake/release of a cargo,[31,32] while anisotropic insertion of a chromophore into a membrane allows spontaneous photoinduced transmem-

[*] K. Liang, Dr. F. Nicoli,[+] Dr. S. A. Shehimy,[+] Dr. S. Di Noja, Y. Li, Dr. C. Bonfio, Dr. G. Ragazzon
Institut de Science et d'Ingénierie Supramoléculaires (ISIS)
University of Strasbourg & CNRS, UMR 7006 8 Allée Gaspard Monge, 67000 Strasbourg, FR
E-mail: ragazzon@unistra.fr

Dr. E. Penocchio
Department of Chemistry
Northwestern University
Evanston, IL 60208, USA

Dr. C. Bonfio, Dr. G. Ragazzon
Strasbourg Institute for Advanced Studies (USIAS)
University of Strasbourg
5 allée du Général Rouvillois, 67000 Strasbourg, FR

Dr. C. Bonfio
Department of Biochemistry
University of Cambridge
Cambridge CB21GA, UK

Dr. S. Borsley
Department of Chemistry
Durham University Lower Mountjoy
Stockton Road, Durham DH1 3LE, UK

[+] These authors are contributed equally.

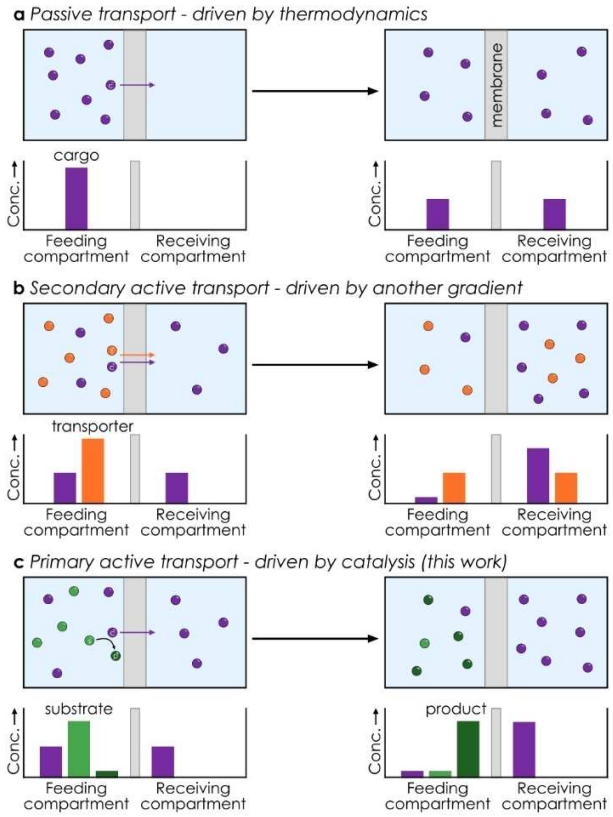

Figure 1. Schematic representation of membrane transport processes. (**a**) Passive transport, where a transmembrane concentration gradient of the cargo is dissipated. (**b**) Secondary active transport, where the transmembrane gradient of a co-transported species is dissipated, providing the energy input for active transport of the cargo. (**c**) Primary active transport, where cargo-mediated catalysis of an orthogonal fuel-to-waste (i. e., substrate to product) reaction results in pumping of the cargo across the membrane, transducing energy from the chemical reaction to generate a concentration gradient.

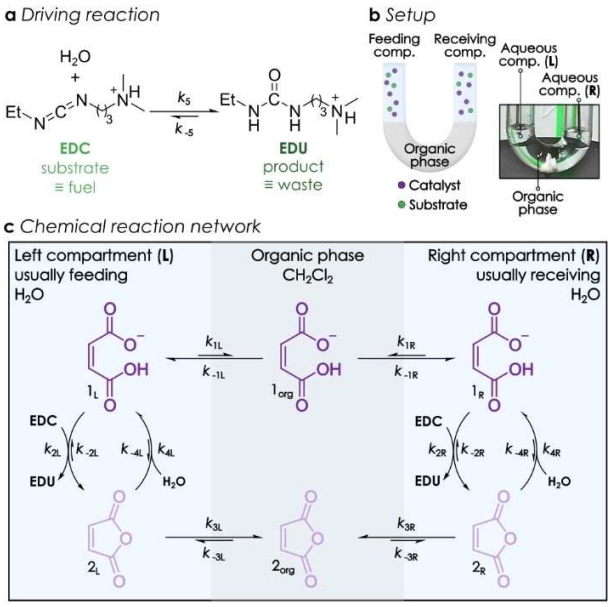

Figure 2. (**a**) Chemical reaction used to provide the energy that drives active transport when catalyzed by maleic acid, i. e., the fuel-to-waste reaction. (**b**) Schematic representation and picture of the experimental setup employed herein: all three phases are stirred simultaneously using mechanical stirrers (top phases) and a magnetic stirrer (bottom phase). (**c**) Chemical reaction network investigated in this work, showcasing the investigated compounds.

brane charge separation, which can drive active transport through charge recombination.[26–28]

In contrast to artificial systems, the majority of biology's active transport processes are chemically powered, often by catalysis of ATP hydrolysis, which transduces chemical energy into transmembrane gradients through catalysis.[10] Realizing this goal in artificial systems would necessitate using catalysis-driven ratchet mechanisms to drive chemical processes other than molecular-level motion.[34] So far, catalysis-driven machines have been used to pump macrocycles onto a collecting chain in a pseudorotaxane,[35] or disequilibrate co-conformational populations in interlocked molecules.[36–38] The conceptual advancement to transfer the principles from small molecules to active transport between macroscopic compartments has just been put forward,[7,33] yet realizing catalysis-driven active transport remains a formidable challenge, explicitly identified by the community.[39]

Here, we describe the catalysis-driven active transport (Figure 1c) of dicarboxylic acid cargoes between aqueous compartments separated by a liquid phase, fueled by the hydration of a carbodiimide (Figure 2a). Diacids are shown to be efficient catalysts for the fuel-to-waste reaction. Transient anhydride formation[40,41] allows passage of the cargo through the hydrophobic layer. We show that localized addition of fuel is sufficient to achieve kinetic asymmetry in the pumping cycle. We further demonstrate that active transport can be achieved through differentiating the anhydride formation and hydrolysis steps, with equal fuel addition in the two compartments. Finally, we offer insights into the thermodynamic and kinetic properties of the process.

Results and Discussion

Design of a Catalysis-Driven Active Transport System

We conducted our investigations in a U-tube set up (Figure 2b), with 2-(*N*-morpholino)ethanesulfonic acid (MES) buffered aqueous compartments (denoted throughout the manuscript as left (**L**), generally the feeding compartment, and right (**R**), generally the receiving compartment) on either side of a dichloromethane liquid phase, which acts as a macroscopic liquid membrane. This set-up is particularly advantageous, as it allows direct sampling of both the aqueous phases and the organic phase by standard ensemble characterization techniques, such as nuclear magnetic resonance (NMR) spectroscopy and high-performance liquid chromatography (HPLC). All three phases were stirred to

ensure efficient mixing of phase boundaries (see Supporting Information, Figure S1 and related text for details).

Several features must be considered in designing an active transport system. (1) How will the cargo be transported across the membrane? For transport between aqueous compartments, the cargo is generally a charged species. To allow passage across a hydrophobic membrane, the charge of the cargo must be temporarily screened or removed. This is a key consideration for both passive and active transport (Figure 1).[42,43] (2) What are the features of the energy source that will drive the active transport? Since active transport is an endergonic process (i. e., has $\triangle G > 0$), it must be driven by an energy-providing process capable of interacting with the cargo to alter its transport kinetics.[7,8] (3) How will anisotropy be provided in the system? The rates of processes must be differentiated on either side of the membrane to determine the direction of active transport and its extent. This can be achieved by differentiating the conditions within the aqueous compartments[7] or by desymmetrizing the membrane itself.[33]

To satisfy these criteria, we selected maleic acid (**1**) as a cargo for active transport. Within a relevant pH range of 5.0–7.0, maleic acid exists predominantly in either the singly or doubly deprotonated form ($pK_a = 1.94$ and 6.22), which prevents passive transport through a hydrophobic phase. We reasoned that the small diacid undergoes a large change in hydrophobicity when converted to maleic anhydride (**2**), since the charge is removed in the anhydride state. This process can be promoted by carbodiimide activation, which has previously proved effective in many systems, in the context of self-assembly,[44–46] autonomous molecular machines,[36–38,47] and even endergonic synthesis.[48,49] In turn, carbodiimide hydration (Figure 2a) takes the role of the "driving reaction": the source of energy. Such a system is mapped by the triphasic chemical reaction network in Figure 2c. Differentiating the composition of the two aqueous phases varies the rate constants for anhydride formation (k_2) or anhydride hydrolysis (k_4),[1] thus introducing kinetic asymmetry to the reaction network, ultimately driving active transport.

Quantification of Isolated Elements of the Reaction Network for Active Transport

All rate constants that describe the reaction network (Figure 2c) can be estimated from simpler experiments examining specific processes in isolation. We first confirmed that maleic acid has a negligible rate of passive transport (i. e., that the pathway from $\mathbf{1_L} \rightarrow \mathbf{1_{org}} \rightarrow \mathbf{1_R}$ via k_{1L} and k_{-1R} is slow). Maleic acid was dissolved in compartment **L** (**L**: $[\mathbf{1}]_0 = 5$ mM, pH_{obs} 6.0, **R**: $[\mathbf{1}]_0 = 0$ mM, pH_{obs} 6.0). We monitored the system by measuring the time-dependent concentration of maleic acid in both the feeding and receiving compartments by HPLC (Figure 3a). A very slight decrease in the concentration of maleic acid in the feeding compartment was observed, while no maleic acid was observed in the receiving compartment over the 3 h course of the experiment. The results indicate that while maleic acid can partially dissolve in the hydrophobic phase, it does not significantly diffuse between the aqueous compartments on the timescale of the experiment.

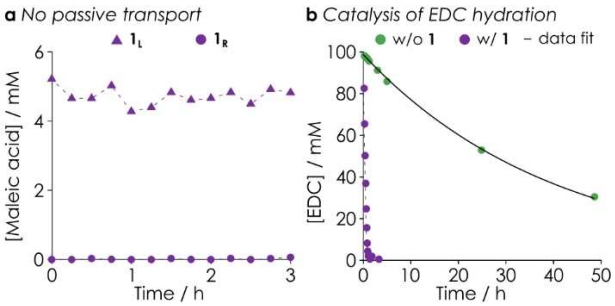

Figure 3. Key preliminary conditions. (**a**) Maleic acid evolution starting from $[\mathbf{1}]_{L,0} = 5$ mM, $[\mathbf{1}]_{R,0} = 0$ mM, monitored by HPLC. (**b**) EDC evolution in time in MES buffer 250 mM, pD_{obs} 6.0 in the presence (purple) or in the absence (green) of 5 mM **1**. The black full line is obtained by fitting the hydration to a first-order process, see Supporting Information, Section S5 for details. Conditions for both panels: [MES] = 250 mM, pH_{obs} 6.0.

We next examined the rate of anhydride hydrolysis in both the aqueous and organic phases. The conversion of maleic anhydride to maleic acid was monitored by ultraviolet-visible (UV/vis) spectroscopy in buffered aqueous solution ($[\mathbf{2}] = 5$ mM, pH_{obs} 6.0), and was well-described by pseudo-first-order kinetics with a half-life of 22 s (corresponding to $k_4 = 0.0319\ s^{-1}$, Figure S4). An analogous experiment was performed in CH_2Cl_2, which had been saturated with the aqueous buffer. In this wet CH_2Cl_2 solution, no appreciable hydrolysis of the anhydride was observed over 17 h ($[\mathbf{2}]_0 = 5$ mM, Figure S6); thus the network in Figure 2c featuring a single cycle[50] is sufficient to describe the system. These experiments suggest that in the triphasic U-tube setup, hydrolysis occurs either at the phase boundaries or in the aqueous phase.

We investigated the competition between phase transfer (k_3) and hydrolysis (k_4) by adding maleic anhydride to compartment **L** only (**L**: $[\mathbf{2}]_0 = 5$ mM, 10 μmol, pH_{obs} 6.0, **R**: $[\mathbf{2}]_0 = 0$ mM, pH_{obs} 6.0, Figure S7). We monitored the appearance of maleic acid in both aqueous phases **L** and **R** by HPLC. A consistent difference of 1.52 μmol in the amount of maleic acid in **L** and **R** phases in favor of $\mathbf{1_L}$ was observed over the entire time-course of the experiment. This difference arises from the competition between hydrolysis (k_4, known, see above) and phase transfer (k_3), hence allowing k_3 to be estimated as $0.018\ s^{-1}$, corresponding to a half-life of 3.8 s, thus faster than the hydrolysis process.

With this information at hand, we studied the partitioning behavior (k_3/k_{-3}) of maleic anhydride by adding it (20 μmol) to the organic phase and monitoring the increase in maleic acid concentration in the aqueous phases following phase transfer and hydrolysis (Figure S8). HPLC analysis immediately after initiation of the experiment detected only

[1] For thermodynamic consistency the microscopic reverse constants, k_{-2} and k_{-4}, are included in the reaction network. However, these values are generally very small due to the large $\triangle G$ of these reactions.

negligible amounts of maleic acid.[2] Since the experiment is performed under vigorous stirring, this observation suggests that the anhydride partitions predominantly into the organic phase. Continued monitoring of the experiment revealed that the total amount of maleic acid in the aqueous phases increased up to 17.8 μmol over time, indicating that about 2.2 μmol, remained in the organic phase ($[\mathbf{1}]_{org.} = 180$ μM, $k_1/k_{-1} = 0.040$) consistent with the observed partitioning of the maleic acid into the organic phase when dissolving it directly in the aqueous phase (Figure 3a).

This experiment indicates that phase transfer from the organic to the aqueous phase (k_{-3}) happens on a suitable timescale, but is not sufficient alone to distinguish between two possible scenarios: either a rapid equilibration of maleic anhydride between the two phases with slower hydrolysis ($k_{-3} \gg k_4$) or a rate-determining phase transfer followed by rapid hydrolysis ($k_{-3} \ll k_4$). To discriminate between these two cases, we built a kinetic model to fit the data obtained in this experiment. Data fitting indicated that phase transfer is rate-determining and followed by rapid hydrolysis (see Supporting Information, Figure S25 and related text).

The remaining process involved in the reaction network is maleic anhydride formation, which was examined first in an isolated aqueous phase. ^{1}H NMR spectroscopy allowed quantification of the carbodiimide-driven conversion of maleic acid to maleic anhydride under the buffered conditions of the experiment ($[\mathbf{1}]_0 = 5$ mM, pD_{obs} 6.0, Figure S9). Upon addition of 100 mM 1-ethyl-3-(3-dimethylaminopropyl)carbodiimide (EDC) to the solution, the first NMR spectrum (t = 3.5 min) already showed maleic anhydride formation, accompanied by conversion of the EDC fuel to 1-ethyl-3-(3-dimethylaminopropyl)urea (EDU) waste. The anhydride persisted until the concentration of EDC was depleted, being hydrolyzed back to maleic acid within ≈50 min (Figure S9). Under these conditions, the half-life of EDC is 16.5 min; this value is almost 90 times shorter than the EDC half-life in the absence of maleic acid (given by k_5, 28 h at pD_{obs} 6.0, Figure 3b), indicating that maleic acid is a good catalyst for EDC hydration, with most of the EDC-to-EDU reactions proceeding via the maleic acid-catalyzed pathway. To gain precise quantitative information on the rate of EDC hydration, we monitored the same experiment (albeit in H_2O instead of D_2O) by UV/vis spectroscopy, which allows monitoring the first few seconds after addition, when anhydride formation is the dominant process (Figure S10). Fitting of the experimental data to a kinetic model afforded $k_2 = 0.37\ M^{-1}s^{-1}$, which implies a half-life of 11 min for EDC in the presence of maleic acid catalyst, in agreement with NMR data.[3]

Together, the experiments examining aspects of the chemical reaction network in isolation confirm (1) the partitioning behavior of both the acid and the anhydride, (2) suitable anhydride formation and hydrolysis rates, and (3) catalysis of the fuel-to-waste reaction. Thus, the maleic acid system fulfills the requirements necessary for performing primary active transport across the macroscopic liquid membrane.

Active Transport Driven by Localized Fuel Addition

To demonstrate active transport within the full system, equimolar concentrations of maleic acid were dissolved in both compartments (**L** = **R**: $[\mathbf{1}]_0 = 5$ mM, pH_{obs} 6.0). EDC (100 mM) was added only to **L** (Figure 4a), and the concentration of species in both aqueous compartments was monitored over time by HPLC (see Supporting Information, Section S2.1). The rapid and complete depletion of maleic acid in compartment **L** was initially observed, confirming the complete partitioning of maleic anhydride into the organic phase. Subsequently, maleic acid concentration gradually increased in compartment **R**, reaching a maximum concentration of 8.9 mM after 4 h, consistent with ≈180 μM

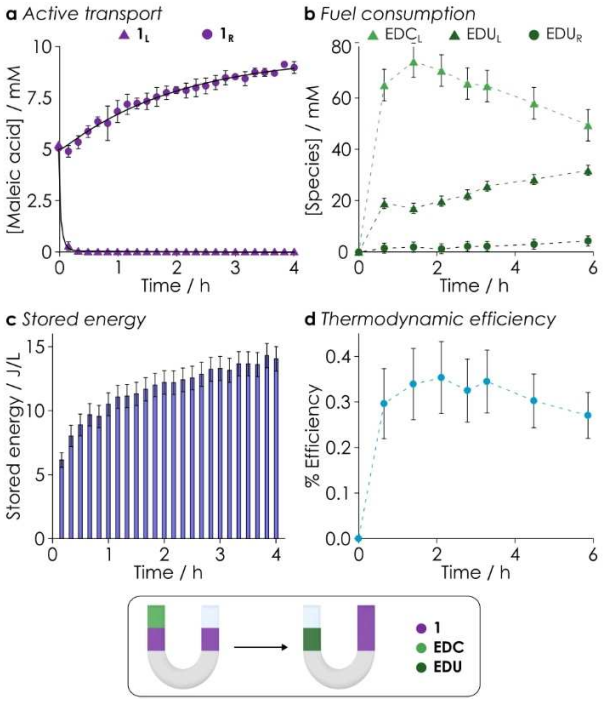

Figure 4. Catalysis-driven active transport. (**a**) Species evolution monitored by HPLC, starting from $[\mathbf{1}]_{L,0} = [\mathbf{1}]_{R,0} = 5$ mM, [MES] = 250 mM pH_{obs} 6.0, with addition of EDC to **L** at t = 0; error bars represent the standard deviation of three independent experiments. The black full lines are obtained by modeling the system using the experimentally determined rate constants. (**b**) The same active transport process as describe in (**a**), with concentrations monitored by NMR and error bars representing the standard deviation associated to the repeated measure of the same sample. (**c**) Evolution of stored energy for the active transport experiment described in panel (**a**). (**d**) Evolution of thermodynamic efficiency, obtained using the NMR-determined concentrations observed in the experiment of panel (**b**). Data refer to the experiment pictured within the box below all panels. See Supporting Information, Sections S2.1, S4.1.3, and S5 for additional details.

[2] We note that maleic anhydride hydrolyzes to maleic acid before HPLC analysis.

[3] The slight discrepancy in the rates determined by ^{1}H NMR and UV/vis spectroscopy may arise from the kinetic isotope affect as a consequence of performing the experiments in D_2O and H_2O respectively, or room temperature differences.

maleic acid remaining dissolved in the organic phase (c.f. Figure 3a). The acidic HPLC analysis conditions employed prevent the concentrations of fuel and waste from being determined. Therefore, we also employed ^{1}H NMR to quantify the evolution of these species. Specifically, we used capillaries to withdraw a few μL of solution for each data point, and transferred the entire capillary to a standard NMR tube for measurement (Figure 4b, see Supporting Information, Section S4.1 for details).

Time-dependent ^{1}H NMR data showed excellent agreement with the HPLC data with respect to the maleic acid concentrations (Figure 4a, c.f. Figure S19), but also showed the maleic acid-catalyzed conversion of EDC-to-EDU as maleic acid is actively transported from **L** to **R**. Specifically, the conversion proceeds to 50 % in ca. 6 h, which is intermediate between the 24 h of the uncatalyzed reaction and the 11 min observed in a homogeneous aqueous phase in the presence of maleic acid catalyst. This decreased rate of hydration compared to the single-phase catalysis experiment is explained by the presence of a negative feedback loop[51] associated with the transport: as the concentration of maleic acid in **L** is depleted, EDC hydration can only occur by the slower, uncatalyzed pathway (k_5). Finally, NMR data show that only a minimal amount of EDU is observed in compartment **R**, which indicates a very limited amount of passive diffusion of either EDC or EDU on the timescale of the experiment, and excludes a role of co-transport phenomena (Figure 1b).

Overall, the results are fully consistent with primary active transport of maleic acid: chemical energy from carbodiimide hydration has been transduced and stored as energy in a chemical gradient of maleic acid across a macroscopic liquid membrane.

The experimentally determined transport data showed excellent agreement with a kinetic model based on the independently measured rate constants (Figure 4a, solid lines, see Supporting Information, Section S5 for details). Modeling reveals that the overall rate of transport is predominantly controlled by the rate of maleic anhydride transfer from the organic to the aqueous phase. Therefore, the model predicts that transfer should be suppressed upon increasing anhydride hydrophobicity. We tested this prediction by performing an identical transport experiment while replacing maleic acid with methylmaleic acid or phthalic acid. In line with model predictions, with methylmaleic acid the rate of active transport is reduced (5.5 mM methylmaleic acid vs 8.5 mM maleic acid observed in the receiving compartment at 3 h), and becomes entirely kinetically suppressed when using phthalic acid (Figure S20, S21). These experiments also demonstrate the generality of the mechanism, which is not solely limited to maleic acid. Furthermore, the generality can be demonstrated even beyond transient anhydride formation. We investigated the chemically-fueled transport of *N*-acetyl-L-histidine, which forms a transient hydrophobic oxazolone upon reaction with EDC.[52] Active transport was successfully achieved, with an increase of [*N*-acetyl-L-histidine] in compartment **R** from 5.0 to 5.9 mM over 24 h, when fueling compartment **L** with 20 mM EDC (Figure S22).

The uneven distribution of maleic acid obtained upon fueling has a higher free-energy content than the initial equilibrium state, which would dissipate if a pathway for passive transport (Figure 1a) became available. The calculation of the free energy stored in chemical disequilibria (chemical potential gradients) is well-established, and can be performed using experimentally measured concentrations.[48,49,53,54] In the present system, the stored energy increases rapidly above 8 J L^{-1} within 25 min, leveling off around 14 J L^{-1} (Figure 4c, see Supporting Information, Section S6 for details). The rapid initial increase is dictated by the fast depletion of maleic acid in **L**, while the subsequent rise is associated with its increase in **R** over time. In fact, these values are lower-bounds for the energy stored, since in compartment **L** the concentration of maleic acid remains below the limit of detection of our analysis method (cf. Figure 4a). The same approach can be used to quantify the input free energy provided to the system by the EDC to EDU conversion.[38,55] This allows estimation of the thermodynamic efficiency of the active transport process as the stored free energy divided by the input free energy. In other words, at any point in time while the transport occurs, the fraction of input free energy that has been effectively stored in form of a concentration gradient can be estimated. The efficiency of the active transport reaches a maximum at ~0.35 % (Figure 4d).

We can appreciate the significance of a 0.35 % efficiency by considering that an ideal mechanism with full directionality would convert one molecule of EDC into EDU while pumping one molecule of maleic acid from one compartment to the other. Taking into account the energetics of these two processes, one retrieves a maximum theoretical efficiency of 3.8 % for pumping all the maleic acid from **L** to **R** using EDC (see Supporting Information, Section S6.1). This value reveals that the reason for a low efficiency lies primarily in the highly exergonic hydration of EDC, which is used to drive a purely entropic energy storage process.[38] Moreover, this experiment is designed to have a statistical 50 % chance of anhydride transfer from the organic to the target aqueous phase, which further lowers to <1.8 % the maximum theoretical efficiency of the process. The further loss of efficiency is due to the slow rate of diffusion of anhydride versus hydrolysis (k_3 vs k_4). This results in anhydride hydrolysis before it has diffused into the organic phase, constituting a futile cycle within the reaction network. While the measured efficiency is five times smaller than the maximum theoretical value of 1.8 %, it nonetheless represents a significant increase in efficiency versus most other systems driven by cabodiimide-hydration reported to date.[48,49] The evolution of efficiency during the course of the experiment presents a bell-shaped profile, offering experimental evidence coherent with a general theoretical prediction on non-equilibrium chemical reaction networks.[56]

Another general theoretical result that can be tested with the present experimental system is the non-equilibrium pumping equality.[57,58] This result predicts that the steady state ratio of any two concentrations, e.g. $[\mathbf{1}]_R/[\mathbf{1}]_L$, is equal the corresponding equilibrium ratio ($[\mathbf{1}]_{R,\,eq}/[\mathbf{1}]_{L,\,eq}=1$) multi-

plied by a kinetic factor.[38] Based on the measured kinetic rate constants in our active transport experiments, we can analytically derive and numerically confirm this general result (see Supporting Information, Section S7.2 for details). The non-equilibrium pumping equality was recently used by Astumian and Sen to describe theoretically a mechanism of chemotaxis.[59] Specifically, they illustrated the case of a catalyst diffusing in a gradient of substrate and product, a situation which closely maps our approach, and inspired it.[7]

Active Transport with Equal Transmembrane Fuel Addition

While the system is directional due to the presence of fuel in only one compartment, selective addition of fuel to a single compartment may not always be possible, e. g., it is hard to imagine fueling only the lumen of a liposome. Therefore, we considered strategies to achieve active transport while fueling both phases. We initially investigated the role of pH, testing active transport at pH values of 5.5 and 6.5 in both compartments, which allows using MES buffer at both pH values, and avoid effects associated with large pH differences.[60] In these conditions, active transport proceeds with a similar rate, extent of transport, and stored energy (Figure S23, S28, S29). This confirms the robustness of the transport mechanism, and further supports a rate-determining role for anhydride phase transfer into water.

Active transport between phases of different pH is also possible. We performed transport experiments across a transmembrane pH gradient, from **L** = pH 6.5 to **R** = pH 5.5 and vice versa. Notably, when driving active transport from the pH 5.5 compartment to the pH 6.5 compartment, the amount of maleic acid accumulated in the receiving compartment is slightly higher than when transport is driven in the opposite direction ($[\mathbf{1}]_R = 8.3$ mM if **R** is at $pH_{obs} = 6.5$ vs $[\mathbf{1}]_R = 6.3$ mM if **R** is at $pH_{obs} = 5.5$, at 2.5 h, Figure S23). Kinetic measurements allowed this observation to be unraveled, revealing that while the half-life for anhydride hydrolysis at pH 5.5 (28.0 ± 0.5 s, Figure S3) is slightly longer than at pH 6.5 (24.5 ± 1.6 s, Figure S5), the activation by EDC is also significantly faster at lower pH, being 0.68 $M^{-1}s^{-1}$ at pD_{obs} 5.5 vs 0.225 $M^{-1}s^{-1}$ at pD_{obs} 6.5, Figure S11, S13). Combining these data, we can calculate an upper limit for kinetic asymmetry of $K_r = 3.9$ (defined counterclockwise with respect of Figure 2c, at t = 0, see Supporting Information, Section S7.1) for the simultaneous fueling of both phases, which indicates that we should observe an accumulation of maleic acid in the compartment at pH 6.5 when fueling both phases with equimolar fuel concentrations. Thus, we performed this experiment, with fuel addition to both **L** and **R** (**L**: $[\mathbf{1}]_0 = 5.3$ mM, pH_{obs} 5.5, $[EDC]_0 = 50$ mM, **R**: $[\mathbf{1}]_0 = 5.3$ mM, pH_{obs} 6.5, $[EDC]_0 = 50$ mM). As predicted, accumulation of maleic acid was observed in the higher pH compartment **R** (Figure 5a). Given the relatively low kinetic asymmetry in this experiment ($K_r = 3.9$ vs essentially unidirectional in localized fueling experiments, c.f. Figure 3), the energy stored is also much lower (0.065 J L^{-1}, see Supporting Information, Figure S30 and related text for the assumptions considered).

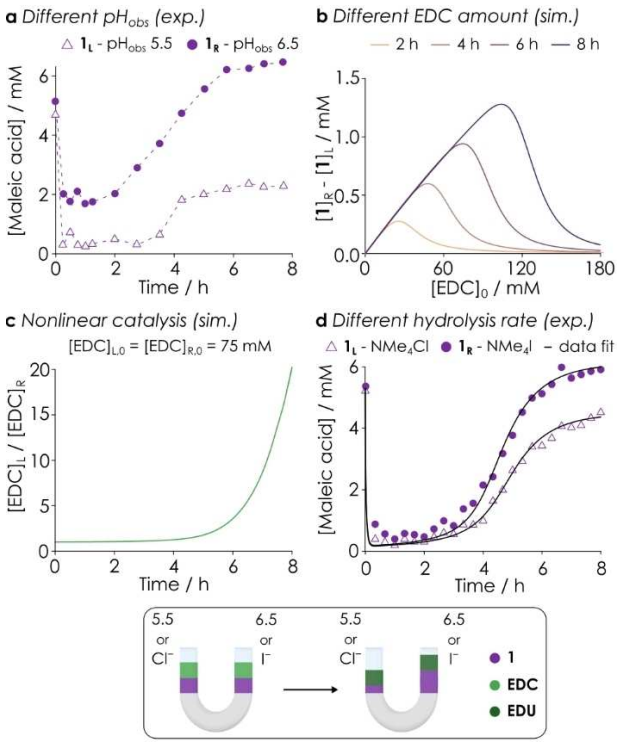

Figure 5. Transport under equal transmembrane fuel addition. (**a**) Evolution of [maleic acid] when fueling compartments having different pH, starting from $[\mathbf{1}]_{L,0} = [\mathbf{1}]_{R,0} = 5$ mM, $pH_{L,obs} = 5.5$, $pH_{R,obs} = 6.5$. and adding simultaneously EDC (50 mM) to both **L** and **R**, at t = 0. (**b**) Simulation of the evolution of the difference in [maleic acid] between compartments **L** and **R**, as a function of $[EDC]_0$, evaluated every 2 h, obtained by fueling with equal EDC amounts on both sides a system where the rate of hydrolysis in compartment **R** is 5% faster than the same process in compartment **L**. (**c**) Evolution of the ratio of [EDC] in compartments **L** and **R**, simulated under the conditions of (**b**) when $[EDC]_0 = 75$ mM. (**d**) Evolution of [maleic acid] when fueling compartments featuring hydrolysis promoter NMe_4I (50 mM) in **R**, and catalytically inert NMe_4Cl (50 mM) in **L**, starting from $[\mathbf{1}]_{L,0} = [\mathbf{1}]_{R,0} = 5.3$ mM, $pH_{L,obs} = pH_{R,obs} = 6.0$, and adding simultaneously EDC (75 mM) to both **L** and **R**, at t = 0. The black full lines are obtained by modeling the system using the experimentally determined rate constants, see Supporting Information, Section S5 for details. Conditions for (**a**) and (**d**): [MES] = 250 mM, species monitored by HPLC. Experimental data refer to the experiment pictured within the box below all panel.

Notably, however, much higher kinetic asymmetry and effectively complete transport can be achieved by operating across a larger pH difference. At pH 9.0 EDC activation is inefficient,[61,62] anhydride hydrolysis is rapid (half-life < 1 s), and transmembrane addition of EDC leads to essentially quantitative transport from pH 5.5 to 9.0 (Figure S24 and related text).

An alternative strategy to impart kinetic asymmetry is to catalytically promote anhydride hydrolysis in one of the compartments. We screened hydrolysis promoters, monitoring transient EDC-promoted maleic anhydride formation in a single phase, in their presence ($[\mathbf{1}]_0 = 5$ mM, [additive] = 50 mM, $[EDC]_0 = 100$ mM, pH_{obs} 6.0). We discovered that both NMe_4Cl and NMe_4I reduce the rate of anhydride

formation (k_2) by about 11 % (possibly due to ion-pair formation between NMe_4^+ andmaleate), while the rate of anhydride hydrolysis (k_4) is ca. 12 % faster in the presence of the iodide salt compared to the chloride (0.0199 s^{-1} for I^- vs 0.0177 s^{-1} for Cl^-, Figure S14, S15).

Our kinetic model allowed us to assess if these small differences are sufficient to provide the anisotropy required to drive appreciable levels of active transport, and to optimize the amount of EDC required. From the simulations, substantial active transport was predicted (>1 mM difference between $[\mathbf{1}]_L$ and $[\mathbf{1}]_R$), even when just a 5 % difference between the hydrolysis rates in the two compartments is present ($k_{4R} = k_{4L} \times 1.05$), provided that enough fuel is present. In particular, larger amounts of EDC extend the lag phase (when maleic acid is mostly in the organic phase), consequently promoting greater accumulation of maleic acid in the receiving compartment **R** (Figure 5b, Figure S26). A factor contributing to the amplification of small differences is that the transport of maleic acid – a catalyst for EDC hydration – simultaneously induces a positive feedback in the compartment **R** (EDC is consumed faster with more maleic acid present) and a negative feedback in compartment **L** (EDC is consumedslower with less maleic acid present), amplifying small imbalances over time. In line with this interpretation, the relative amount of EDC in compartment **L** (i. e., $[EDC]_L/[EDC]_R$) becomes progressively larger, increasing nonlinearly over time (Figure 5c). In turn, kinetic asymmetry is increased favoring directional transport.

Building on these insights, we performed active transport experiments adding hydrolysis promoter NMe_4I (50 mM) in compartment **R**, and inactive NMe_4Cl (50 mM) to compartment **L** to ensure a balance of salt concentration and account for any thermodynamic effects. The conditions across the two compartments were otherwise identical, with the same pH and a substantial amount of fuel added (both **L** and **R**: $[\mathbf{1}]_0 = 5$ mM, pH_{obs} 6.0, $[EDC]_0 = 75$ mM, $[NMe_4X] =$ 50 mM, with X = Cl in **L** and X = I in **R**.). Active transport was observed, with accumulation of a nonequilibrium concentration of maleic acid in **R**, the compartment bearing hydrolysis promoter NMe_4I (Figure 5d), with the final maleic acid concentrations determined as $[\mathbf{1}]_L = 4.3$ mM, $[\mathbf{1}]_R = 5.8$ mM. The kinetic asymmetry at t = 0 under these conditions is 1.17, though notably this value increases over time due to feedback (see Supporting Information Section S7), while the energy stored goes up to 0.4 J L^{-1}. While the extent of transport is relatively small compared to those obtained by localized fuel addition, the resulting gradient of maleic acid is comparable or even greater with respect to those achieved in the most advanced light-driven systems.[31,32]

The two experiments employing either a transmembrane pH gradient or addition of NMe_4I as hydrolysis promoter (Figure 5a,d) provide a crucial demonstration that active transport can be achieved even when fuel is present in equimolar concentrations on both sides of a macroscopic membrane: selectivity can be obtained within the chemical reaction network reported herein by differentiating the rate of anhydride formation and/or hydrolysis between the two compartments, leveraging simultaneous autocatalysis and negative feedback.

Conclusion

In summary, we have successfully achieved primary active transport powered by chemical energy, transducing energy through catalysis for the generation of a transmembrane molecular gradient. Control of the relative rates of anhydride formation and hydrolysis of a maleic acid cargo on either side of a macroscopic liquid membrane provides kinetic asymmetry,[6–8,18,34] driving active transport in a fully artificial system. The anisotropy for determining the direction of transport is provided by differentiating the conditions within the aqueous compartments. Most simply, this can be provided by adding fuel to only one compartment. However, we demonstrate that, even when equimolar fuel is present in both aqueous compartments, pH differences or catalytic acceleration of hydrolysis can afford the anisotropy required to provide kinetic asymmetry and drive the formation of a concentration gradient. In the terminology proper of artificial molecular machines, the system can be doubly kinetically gated.[36,63]

Most notably, this research leverages the principles of molecular ratchets, translating concepts from small molecule machines to a transmembrane setting.[7,8,33] While the molecules and mechanism appear very different to their small molecule counterparts, the active transport we have demonstrated is driven by fundamentally the same type of catalysis-driven information ratchet as has been demonstrated for small molecule motors and pumps, underpinning most biomolecular machines,[10] and more broadly disequilibria conversion.[64] This is further supported by kinetic modelling, where rate constants measured in isolated systems can be combined to fully model the reaction network – with predictive ability. Remarkably, we demonstrated the emergence of nonlinear phenomena such as autocatalysis and negative feedback in a simple kinetically asymmetric network, connecting ratchet mechanisms with nonlinear systems.[65] Here, active transport of maleic acid catalyzes EDC hydration in the receiving compartment, while simultaneously producing a negative feedback in the feeding compartment: a dual nonlinear effect reminiscent of the mechanism at the basis of Soai reaction.[66,67] Key challenges still need to be addressed to translate this mechanism to lipid membranes (See Supporting Information, Section 8); however, the extension of active transport to pump an amino acid such as *N*-acetyl-L-histidine, achieved by leveraging a different reaction cycle[52] indicates that our approach is suitable to further extension. By offering a first example of bioinspired catalysis-driven active transport in artificial systems, our work offers a new approach to the design and development of life-inspired nanotechnologies.[68]

Supporting Information

The Supporting Information is available free of charge: experimental methods and setup, additional data discussed in the main text, details of theoretical analysis.

Acknowledgements

This work has benefitted from support provided by two entities within the French National program "investments for the future IdEx Unistra (ANR-10-IDEX-0002): the Interdisciplinary Thematic Institute ITI-CSC, and the University of Strasbourg Institute for Advanced Study (USIAS) for two Fellowships. Additional support was received by the European Research Council (ERC-2021-StG 101041933 – KI-NET to G. R.) and the Chinese Scholarship Council. S.B. is a Royal Society University Research Fellow. The authors thank Cyril Antheaume, Arthur Schmitt, Fabiana Ciocchetti, and Ahmad Bachir for their help in preliminary experiments and analytical measurements, Lucia Pasquato for fruitful discussions, and Job Boekhoven and co-authors for openly discussing their related findings.[69]

Conflict of Interest

The authors declare no conflict of interest.

Data Availability Statement

The data that support the findings of this study are available in the supplementary material of this article.

Keywords: active transport · molecular ratchets · kinetic asymmetry · systems chemistry · chemical fuel

[1] N. A. Yewdall, A. F. Mason, J. C. M. van Hest, *Interface Focus* **2018**, *8*, 20180023.
[2] C. T. Walsh, B. P. Tu, Y. Tang, *Chem. Rev.* **2018**, *118*, 1460–1494.
[3] F. H. Westheimer, *Science* **1987**, *235*, 1173–1178.
[4] D. L. Nelson, M. Cox, *Lehninger Principles of Biochemistry*, W. H. Freeman, New York, NY, USA, **2017**.
[5] E. R. Kay, D. A. Leigh, F. Zerbetto, *Angew. Chem. Int. Ed.* **2007**, *46*, 72–191.
[6] R. D. Astumian, *Nat. Commun.* **2019**, *10*, 3837.
[7] T. Sangchai, S. Al Shehimy, E. Penocchio, G. Ragazzon, *Angew. Chem. Int. Ed.* **2023**, *62*, e202309501.
[8] S. Borsley, B. M. W. Roberts, D. A. Leigh, *Angew. Chem. Int. Ed.* **2024**, *63*, e202400495.
[9] S. Borsley, D. A. Leigh, B. M. W. W. Roberts, *Nat. Chem.* **2022**, *14*, 728–738.
[10] M. Schliwa, G. Woehlke, *Nature* **2003**, *422*, 759–765.
[11] E. Racker, *Trends Biochem. Sci.* **1976**, *1*, 244–247.
[12] P. J. Garrahan, I. M. Glynn, *Nature* **1966**, *211*, 1414–1415.
[13] R. Dipolo, *Nature* **1978**, *274*, 390–392.
[14] K. P. Locher, *Nat. Struct. Mol. Biol.* **2016**, *23*, 487–493.
[15] C. Thomas, R. Tampé, *Annu. Rev. Biochem.* **2020**, *89*, 605–636.
[16] O. Jardetzky, *Nature* **1966**, *211*, 969–970.
[17] R. D. Astumian, P. B. Chock, T. Y. Tsong, H. V. Westerhoff, *Phys. Rev. A* **1989**, *39*, 6416–6435.
[18] R. D. Astumian, M. Bier, *Biophys. Chem.* **1996**, *70*, 637–653.
[19] R. D. Astumian, S. Mukherjee, A. Warshel, *ChemPhysChem* **2016**, *17*, 1719–1741.
[20] B. Alberts, *Molecular Biology of the Cell*, W. W. Norton & Company, New York, NY, USA, **2015**.
[21] J. H. Moore, R. S. Schechter, *Nature* **1969**, *222*, 476–477.
[22] J.-P. Behr, J.-M. Lehn, *J. Am. Chem. Soc.* **1973**, *95*, 6108–6110.
[23] T. Shinbo, K. Kurihara, Y. Kobatake, N. Kamo, *Nature* **1977**, *270*, 277–278.
[24] J. J. Grimaldi, J.-M. Lehn, *J. Am. Chem. Soc.* **1979**, *101*, 1333–1334.
[25] E. N. W. Howe, P. A. Gale, *J. Am. Chem. Soc.* **2019**, *141*, 10654–10660.
[26] G. Steinberg-Yfrach, P. A. Liddell, S. C. Hung, A. L. Moore, D. Gust, T. A. Moore, *Nature* **1997**, *385*, 239–241.
[27] I. M. Bennett, H. M. Vanegas Farfano, F. Bogani, A. Primak, P. A. Liddell, L. Otero, L. Sereno, J. J. Silber, A. L. Moore, T. A. Moore, D. Gust, *Nature* **2002**, *420*, 398–401.
[28] S. Bhosale, A. L. Sisson, P. Talukdar, A. Fürstanberg, N. Banetji, E. Vauthey, G. Bollot, J. Mareda, C. Röger, F. Würthner, N. Sakai, S. Matile, *Science* **2006**, *313*, 84–86.
[29] T. L. Longin, M. L. Goyette, C. A. Koval, *Chem. Innovation* **2001**, *31*, 23–30.
[30] X. Xie, G. A. Crespo, G. Mistlberger, E. Bakker, *Nat. Chem.* **2014**, *6*, 202–207.
[31] J. Pruchyathamkorn, B. N. T. Nguyen, A. B. Grommet, M. Novoveska, T. K. Ronson, J. D. Thoburn, J. R. Nitschke, *Nat. Chem.* **2024**, *16*, 1558–1564.
[32] B. Shao, H. Fu, I. Aprahamian, *Science* **2024**, *385*, 544–549.
[33] S. Borsley, *ChemSystemsChem* **2024**, *6*, e202400004.
[34] G. Ragazzon, L. J. Prins, *Nat. Nanotechnol.* **2018**, *13*, 882–889.
[35] S. Amano, S. D. P. Fielden, D. A. Leigh, *Nature* **2021**, *594*, 529–534.
[36] S. Borsley, D. A. Leigh, B. M. W. Roberts, *J. Am. Chem. Soc.* **2021**, *143*, 4414–4420.
[37] S. Borsley, D. A. Leigh, B. M. W. Roberts, I. J. Vitorica-Yrezabal, *J. Am. Chem. Soc.* **2022**, *144*, 17241–17248.
[38] L. Binks, S. Borsley, T. R. Gingrich, D. A. Leigh, E. Penocchio, B. M. W. Roberts, *Chem* **2023**, *9*, 2902–2917.
[39] M. J. Langton, *Nat. Chem. Rev.* **2021**, *5*, 46–61.
[40] S. A. P. Van Rossum, M. Tena-Solsona, J. H. Van Esch, R. Eelkema, J. Boekhoven, *Chem. Soc. Rev.* **2017**, *46*, 5519–5535.
[41] L. S. Kariyawasam, C. S. Hartley, *J. Am. Chem. Soc.* **2017**, *139*, 11949–11955.
[42] A. P. Davis, D. N. Sheppard, B. D. Smith, *Chem. Soc. Rev.* **2007**, *36*, 348–357.
[43] S. Matile, A. V. Jentzsch, J. Montenegro, A. Fin, *Chem. Soc. Rev.* **2011**, *40*, 2453–2474.
[44] B. Rieß, R. K. Grötsch, J. Boekhoven, *Chem* **2020**, *6*, 552–578.
[45] L. S. Kariyawasam, M. M. Hossain, C. S. Hartley, *Angew. Chem. Int. Ed.* **2021**, *60*, 12648–12658.
[46] X. Chen, M. A. Würbser, J. Boekhoven, *Accounts Mater. Res.* **2023**, *4*, 416–426.
[47] S. Borsley, E. Kreidt, D. A. Leigh, B. M. W. Roberts, *Nature* **2022**, *604*, 80–85.
[48] E. Olivieri, J. M. Gallagher, A. Betts, T. W. Mrad, D. A. Leigh, *Nat. Synth.* **2024**, *3*, 707–714.
[49] S. Al Shehimy, H.-D. Le, S. Amano, S. Di Noja, L. Monari, G. Ragazzon, *Angew. Chem. Int. Ed.* **2024**, *63*, e202411554.
[50] E. Penocchio, A. Bachir, A. Credi, D. Astumian, G. Ragazzon, *Chem* **2024**, *10*, 3644–3655.
[51] O. Brandman, T. Meyer, *Science* **2008**, *322*, 390–395.

[52] X. Chen, M. Stasi, J. Rodon-Fores, P. F. Großmann, A. M. Bergmann, K. Dai, M. Tena-Solsona, B. Rieger, J. Boekhoven, *J. Am. Chem. Soc.* **2023**, *145*, 6880–6887.
[53] S. Corra, M. T. Bakić, J. Groppi, M. Baroncini, S. Silvi, E. Penocchio, M. Esposito, A. Credi, *Nat. Nanotechnol.* **2022**, *17*, 746–751.
[54] T. Marchetti, L. Gabrielli, D. Frezzato, L. J. Prins, *Angew. Chem. Int. Ed.* **2023**, *62*, e202307530.
[55] F. Tordini, A. Bencini, M. Bruschi, L. De Gioia, G. Zampella, P. Fantucci, *J. Phys. Chem. A* **2003**, *107*, 1188–1196.
[56] E. Penocchio, R. Rao, M. Esposito, *Nat. Commun.* **2019**, *10*, 3865.
[57] R. D. Astumian, B. Robertson, *J. Am. Chem. Soc.* **1993**, *115*, 11063–11068.
[58] R. D. Astumian, *Acc. Chem. Res.* **2018**, *51*, 2653–2661.
[59] N. S. Mandal, A. Sen, R. D. Astumian, *J. Am. Chem. Soc.* **2023**, *145*, 5730–5738.
[60] I. J. Colton, R. J. Kazlauskas, *J. Org. Chem.* **1994**, *59*, 3626–3635.
[61] I. T. Ibrahim, A. Williams, *J. Am. Chem. Soc.* **1978**, *100*, 7420–7421.
[62] P. S. Schwarz, M. Tena-Solsona, K. Dai, J. Boekhoven, *Chem. Commun.* **2022**, *58*, 1284–1297.
[63] S. Amano, M. Esposito, E. Kreidt, D. A. Leigh, E. Penocchio, B. M. W. Roberts, *J. Am. Chem. Soc.* **2022**, *144*, 20153–20164.
[64] E. Branscomb, T. Biancalani, N. Goldenfeld, M. Russell, *Phys. Rep.* **2017**, *677*, 1–60.
[65] S. Amano, S. Borsley, D. A. Leigh, Z. Sun, *Nat. Nanotechnol.* **2021**, *16*, 1057–1067.
[66] K. Soai, T. Shibata, H. Morioka, K. Choji, *Nature* **1995**, *378*, 767–768.
[67] D. G. Blackmond, *Proc. Natl. Acad. Sci. USA.* **2004**, *101*, 5732–5736.
[68] B. A. Grzybowski, W. T. S. Huck, *Nat. Nanotechnol.* **2016**, *11*, 585–592.
[69] C. M. E. Kriebisch, B. A. K. Kriebisch, G. Häfner, Y. Fei, M. Müller, J. Boekhoven, *ChemRxiv.* **2024**, DOI: 10.26434/chemrxiv-2024-4rk8f.

Manuscript received: November 1, 2024
Accepted manuscript online: February 7, 2025
Version of record online: ■■, ■■

Forschungsartikel

Systems Chemistry

K. Liang, F. Nicoli, S. A. Shehimy, E. Penocchio, S. Di Noja, Y. Li, C. Bonfio, S. Borsley, G. Ragazzon* ___ **e202421234**

Catalysis-driven Active Transport Across a Liquid Membrane

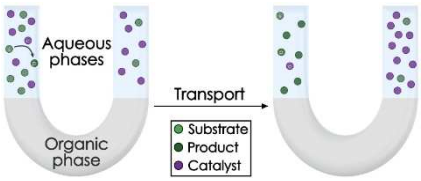

We describe how a small-molecule catalyst can be transported against its concentration gradient, thanks to the energy provided by the chemical reaction it catalyzes. This non-equilibrium process builds macroscopic concentration gradients and can be triggered by the localized presence of co-catalysts. Spatial separation leads to simultaneous autocatalysis and negative feedback, connecting the worlds of molecular ratchets and nonlinear phenomena.